Citation
Shi, T. and Zhang, X. and Hao, H. and Chen, C. 2021. Experimental and numerical investigation on the compressive properties of interlocking blocks. Engineering Structures. 228: ARTN 111561.
http://doi.org/10.1016/j.engstruct.2020.111561

Experimental and numerical investigation on the compressive properties of interlocking blocks

Tingwei Shi, Xihong Zhang*, Hong Hao, Chong Chen

Centre for Infrastructural Monitoring and Protection, School of Civil and Mechanical Engineering, Curtin University

Abstract

Masonry construction with interlocking bricks could effectively reduce construction time, minimize labour cost and improve construction quality. Existing interlocking bricks are mostly designed to provide easy alignment only, therefore the effect of interlocking mechanism on the mechanical performance of the interlocking block is not well investigated. This paper presents a laboratory and numerical study on the mechanical properties of a new type of interlocking brick featured with large shear keys for better mechanical performance. The theoretical compressive strength of a unit brick prism is derived using fracture mechanics theory, which is validated with laboratory compression test. Then, further tests on prisms with multiple interlocking bricks show the number of bricks strongly influences the performance of prism compressive strength. Detailed 3D numerical models of interlocking brick prisms are generated using ABAQUS. The numerical modelling results are compared with experimental test results. The damage and failure modes of the interlocking blocks are numerically and experimentally studied. Localized stress concentration at block interlocking surfaces is investigated. Parametric study is then carried out to quantify the influences of different design parameters including the number of blocks, brick surface roughness amplitude due to brick manufacturing tolerance and surface unevenness, and material strength. A modified formula based on the analytical solution is derived by fitting the numerical simulation and experimental results to predict the compressive capacity of interlocking brick prisms. A semi-empirical prediction method is also derived to predict the axial stiffness of the interlocking brick prism for use in design analysis of masonry structures made of mortar-less interlocking bricks.

Keywords: Interlocking brick, mortar-less, dry-stacking, contact imperfection, numerical modelling

1. Introduction

Masonry structure is one of the most predominant structures throughout the world particularly for low-rise residential structures. This is mainly because of its relatively low cost comparing with reinforced concrete and steel structures, outstanding thermal and sound insulation performance, and robust structural performance in comparison to timber and other structures. Conventional masonry construction comprises of clay bricks bonded together by a layer of mortar or cementitious material. Because of the relatively low strength of mortar, failure in conventional masonry structures always initiates in the mortar or at the bonding interfaces with bricks. Conventional masonry structures normally exhibit poor structural performance particularly against extreme loading conditions such as earthquake, impact and blast loads. For example, Giamundo et al [1] carried out shaking tables tests on a full-scale unreinforced brick masonry vault and found that interfaces between mortar and brick were the weakest part of the vault where crack opening and closing occurred. In the meanwhile, many old and historical constructions built with mortar and bricks show a serious loss of structural performances because of chemical, physical, and mechanical degradation of the mortar layer [2, 3]. In addition, the construction efficiency and structure quality are very much dependent on the competency and experience of brick layers.

Considering the above deficiencies, the advancements of masonry structures in the past decades include (but not exclusively) introducing thin-bed or mortar-less (dry-stacking) construction methods to improve construction efficiency, and using interlocking bricks to replace conventional plain bricks in order to improve structure mechanical performance. Combining the above features, dry-stacking interlocking masonry blocks could lead to significant reductions in construction time, minimization of labour cost, increase in the shear resistance [4, 5] and improvement of the construction quality [6-9], which therefore have attracted a lot of interests from the construction industry, and have been more and more popularly used in practice.

Various types of interlocking bricks have been developed to improve construction efficiency and quality [9-17]. Anand and Ramamurthy discussed the development of available interlocking bricks [18]. It was reported that the production rate with interlocking brick could be 2.5~5 times higher than conventional brick, and 60%~80% labour saving during construction by employing interlocking bricks [19]. Apart from the great construction efficiency and quality that can be achieved by using interlocking bricks, the requirement on competence and experience of construction workers could be substantially relieved as the interlocking mechanism of bricks can help to ensure alignment. Without using relatively weaker mortar layer could also enhance the robustness and strength of the masonry structure. These features are also found to suit particularly to most rural areas where skilled labours for conventional brick construction are in shortage which leads to shabby structure quality and vulnerable structures especially when facing nature disasters [20].

Different interlocking mechanisms were introduced over the past few years. The interlocking mechanism can be provided in either horizontal, vertical or both directions. Plate-like assemblies of tetrahedral or osteomorphic bricks were also proposed in recent studies [5]. The mechanical performances of brick with different interconnections were experimentally investigated by different researchers. For example, with direct shear tests on interlocking bricks comprising two shallow truncated cones, Sturm et al. [7] proved the effectiveness of shear key in improving the shear resistance capacity with the damage to tenons being observed in the tests. It shall be noted that most current designs of interlocking brick systems are featured with small shear keys for construction easiness. Because the projection area of the shear tenon is relatively small, the shear resistance between interlocking blocks is therefore not significantly improved [21]. Faidra et al. [22] investigated interlocking assemblies of glass components with imperfect contacts. It was found that the osteomorphic blocks showed good multifunctionality and the dry-stacked glass columns could still carry a considerable amount of compressive load after some of the components were broken. Recently, some researchers carried out preliminary tests on interlocking connections with large tenon and mortise to improve the shear resistance, damages to the tips of tenon and mortise were observed when the bricks were under low axial compression; and failure mode of tenon total shear off was found when the applied axial force was large [23, 24]. The influence of interlocking connection on brick axial loading capacity was also studied, mainly by experimental tests [25, 26]. Some researchers found low axial loading capacity of interlocking bricks because of the relatively small contact area due to joint imperfection [27, 28]. Crack and failure of stacked pier with interlocking bricks initiated from the mortise of the connection due to lateral expansion and stress concentration [14, 18, 29, 30]. Studies on the flexural bending capacity of interlocking brick are rare because without axial pre-compression, no bending resistance could be provided by mortar-less interlocking bricks. Some preliminary laboratory tests found that when prestress was applied, similar flexural bending capacity was reported as compared to conventional brick with prestress [31]. Recent studies by Zhang et al. observed stress concentration of columns made of concrete blocks with shear keys under cyclic loading, which could cause concrete crushing damage and hence reduce the column capacity to resist seismic loading [32-37]. There is still a lack of systematic study on the mechanical properties of interlocking brick structures.

Mortar-less (dry-stacking) block is to lay masonry units without using any mortar layers. The elimination of mortar obviously reduces material cost and enables cold weather construction to proceed through the winter months with much less elaborated requirements for weather protection. Dry-stacking method could also eliminate the problem of shrinkage cracking in concrete masonry units, and most important of all it requires much less skilled and experienced labour forces which can be a major advantage in light of the shortage of skilled labours. It also increases the productivity and speed of construction. All of these advantages translate into greater economy for the system while maintaining the inherent characteristics of masonry construction [19, 38, 39]. Despite all those advantages, the mechanical performance of dry-stacking masonry blocks is largely influenced by the geometric imperfection of the blocks as a result of the contact surface imperfection [28, 40, 41]. Since clay bricks are normally manufactured in kiln, the high temperature burning of extruded clay mixture process leads to irregular brick surface topography and unit height difference (irregular surface topology) of up to a few millimetres. For conventional brick-laying method with thick mortar layer (approximately 10 mm), the effects of brick height difference and irregular surface topography at the connections can be moderated by mortar. For mortar-less method, the influence of brick geometric imperfection on its mechanical properties cannot be ignored. Casapulla and Portioli [42] experimentally investigated the contact behaviour at the interface between dry-stacked masonry blocks, and found the joint behaviour of two rough blocks passing over each other was strongly dependent on surface roughness. Agaajani [41] discovered that the height of manufactured blocks followed a Gauss statistical distribution, which thereby caused an indubitably height variation when blocks are aligned in a wall. Jaafar et al. [28] examined the height difference (± 0.25 mm) of a batch of blocks from local major brick manufacturers and conducted compressive tests on dry-stacking brick prisms. It was found that the difference of compressive displacement at different locations in the same plane section of the prism can be up to 0.90 mm. This is mainly due to variation in the behaviour of contact at the dry joints. This difference in compressive displacement could result in internal shear stress which leads to reduced prism compressive strength. Despite the absolute value of surface imperfection appears to be small, these imperfections on the joints could lead to stress concentration in the block connections and therefore decrease the ultimate load-carrying capacity of a masonry system. The contact behaviour at the interface between the dry-stacked masonry blocks is also affected by micro-scale phenomena, including cohesion, contact pressure and friction [21, 27, 43-46]. Bosro et al. [47] modelled the interface properties between the blocks using surface to surface contact with a friction coefficient of 0.603. Ayed et al. [27] used Coulomb friction criterion to describe failure of the interface between blocks through the numerical model which considered the linear elastic behaviour of the material and ignored the material non-linear behaviour. Zahra and Dhanasekar [44] generated a micro-scale finite element model to simulate the rough surfaces of the dry-stacking interface by adjusting the location of the nodal coordinate and assigning rock properties to the peaks at the bed joints. Several other researchers [14, 48-51] also emphasised that the ultimate load-carrying capacity obtained by a dry-stacking masonry prisms was significantly dependent on the extent of imperfection at the dry interface. Some studies investigated the contact behaviour of dry-stacking bricks, and examined its influence on the overall behaviour of masonry systems [17]. For example, Zahra et al. [52] used matrix based tactile surface sensors (MBTSS) to obtain the contact area and contact pressure of the dry-stacking brick prism under compression. Rekik et al. [25] employed non-contact digital image correlation (DIC) technique to ascertain both the contact area and the contact pressure. Zahra et al. [52] used carbon paper image imprints to trace the loading increments, and each imprint was then analysed to find out the contact surface area. The contact surface of mortar-less brick system was also simplified into a two-dimensional numerical model by some researchers [26, 53, 54]. However, the simplified 2D model could not capture cracks occurring out of the plane. Ngapeya et al. [2] generated a 3D model of dry-stacking blocks, and studied the influence of block height imperfection on the axial load-carrying capacity of prism. Comparison was also made between analytical approaches and their finite element analyse results. Mousavian and Casapulla [55] extended the limit analysis method with a concave contact model for the interlocking interfaces to design structurally feasible assemblages of interlocking blocks. These above studies demonstrated that for dry-stacking masonry construction, block geometric imperfection caused by surface topography and brick height variation could lead to significant mechanical performance variation [56-58]. For engineering application, it is critical to properly study the influence of the contact surface on the stiffness characteristics, stress concentration and failure modes of the dry-stacking masonry system. Until now, there is no study yet about the influences of surface unevenness of interlocking bricks on properties of masonry structures.

For mortar-free interlocking brick system, the interlocking blocks could move slightly if the interlocking joint is not perfectly closed and tight when it is subjected to in-plane shear load. This relative movement could help to improve energy dissipation of the brick system under lateral loads. Because of the shear resistance from the inclined keys, these interlocking blocks could exhibit better self-centring capacity. The lack of bedding mortar also removes the lateral tensile stresses in masonry blocks, which initiates early splitting at a low stress level when masonry is subjected to axial compression [18]. Since the interlocking mechanism of mortar-less connection differs significantly from conventional mortar connection, the current understandings about the mechanical behaviour of the conventional masonry structures could not be simply adopted to analyse and design the masonry structures with interlocking bricks.

This study employs analytical derivation, experimental testing and numerical modelling to study the compressive properties of mortar-less interlocking brick system. The structure of this paper is as below: First, the configuration of the interlocking brick and the theoretical compressive strength of a unit brick are presented. Laboratory compression test is then carried out to validate the theoretical derivation, as well as further tests on interlocking prisms with multiple bricks. Detailed numerical models are then built. The results including the compressive load versus axial displacement curves, crack initiation and development, and prism damage and failure modes, are compared between the numerical simulation and laboratory test results. Parametric study is then carried out to quantify the influences of the number of bricks, brick surface roughness amplitude due to brick manufacturing tolerance and surface evenness, and brick material compressive strength. A modified design formula based on the analytical solution, laboratory and numerical results is derived to predict the compressive strength of interlocking brick prisms. Last but not the least, a semi-empirical formula is proposed to predict the compressive stiffness of the interlocking brick prism.

2. Interlocking bricks

2.1 Brick configuration

Figure 1 illustrates the configuration of the interlocking blocks of dimension 200 mm ×180 mm ×100 mm (length ×height ×thickness). As shown, the blocks have large protruded mortise and tenon of dimension 35 mm length × 30 mm height × 35 mm thickness. This is different from other existing interlocking blocks that usually have small keys primarily for alignment only rather than resisting shear force. The tenons are inclined, which enable the assembled blocks to slide under lateral loading. The blocks are made of cement, sand and gravel through high pressure moulding, therefore have concrete-like constitutive properties.

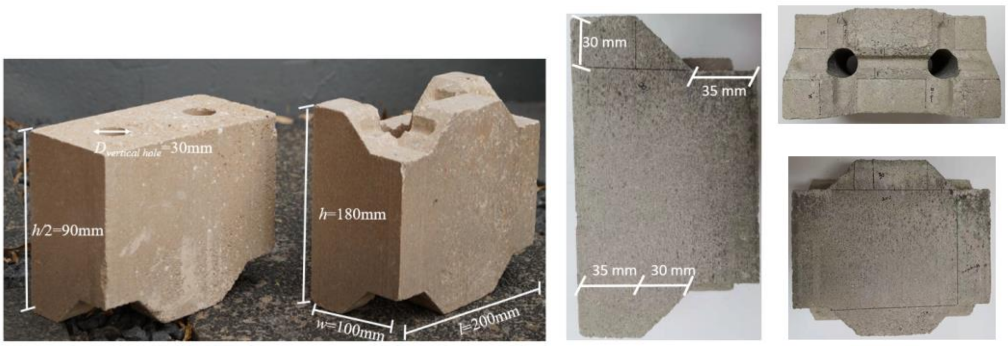

Figure 1. Configuration of interlocking blocks

2.2 Theoretical compressive strength

With the introduction of interlocking keys to the joint, the compressive load-carrying capacity of brick prisms made of interlocking bricks could be influenced. Fracture mechanics theory is employed to analyse the compressive strength of interlocking brick prism. A one-block prism comprising of a full interlocking brick and two half bricks as shown in Figure 2 is taken as the fundamental unit for analysis here.

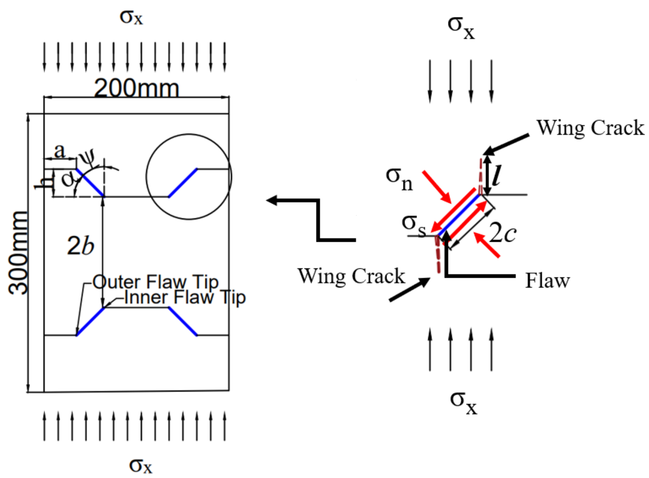

Figure 2. Illustration of force analysis of a fundamental unit

The compressive force on the prism produces vertical stress across the interlocking joint. When acting on the inclined section of the shear key ($2c$), the vertical stress can be decomposed to a normal and a shear component as shown in Figure 2, delamination could be triggered due to the normal component. Taking this delamination as a 'pre-existing' flaw, a shear crack could further develop at its tips, whose faces slide under shear stress $\tau = \sigma_x(\sin\alpha\cos\alpha - \tan\varphi cos^2\alpha)$, where σ_x is the compressive stress, and the expression represents the shear stress induced on the plane of the contact interface minus the frictional stress (cohesion is ignored) [5]. If the effective shear stress is high enough to endure the frictional stress along the closed inclined interlocking key, the frictional sliding will result in tensile stress concentrations at the flaw tips of the interlocking key, therefore trigger the initiation and propagation of the wing cracks that are mainly induced by a high shear stress concentration in the bridge area and coalescence [59, 60]. For the one-block prism shown in Figure 2, there are four flaws on the front elevation view of the prism. According to the hypothesis proposed by Wong and Chau [61], the ultimate strength of flawed specimens is not influenced by the total number of pre-existing flaws, but only by the geometric shape of the interlocking brick. The total stress intensity factor K_I for the growth of wing cracks can be expressed as:

$$\frac{K_{\mathrm{I}}}{\sigma_x\sqrt{\pi c}} = \frac{\left(sin2\psi - \mu + \mu cos2\psi\right)}{(1+L)^{\frac{3}{2}}}\left[0.23L + \frac{1}{\sqrt{3}(1+L)^{\frac{1}{2}}}\right] + \left[\frac{2\varepsilon_0(L+cos\psi)}{\pi}\right]^{\frac{1}{2}} \tag{1}$$

where ψ is the angle calculated from the σ_x-direction to the direction along the flaw surface (i.e. ψ=90°−α), 2c denotes the length of the pre-existing flaw, $L=l/c$ stands for the normalized length of the wing cracks (l denotes the length of the growth of wing crack), μ is the frictional coefficient along the frictional or shear flaw, and the flaw density ε_0 is measured from Nc^2/A (N is defined as the number of flaw for an unit area A). Wing cracks initiate when $K_{\mathrm{I}} = K_{\mathrm{IC}}$, where K_{IC} denotes the fracture toughness of the material of the brick [5, 62]. And hence the maximum compressive strength $\sigma_x^{\max}$ of a flawed prism can be expressed as:

$$\sigma_1^{max} = \frac{K_{IC}}{\sqrt{\pi c}}\left\{\frac{[sin2\psi - \mu + \mu cos2\psi]}{(1+L_{cr})^{\frac{3}{2}}} \times \left[0.23L_{cr} + \frac{1}{\sqrt{3}(1+L_{cr})^{\frac{1}{2}}}\right] + \left[\frac{2\varepsilon_0(L_{cr}+cos\psi)}{\pi}\right]^{\frac{1}{2}}\right\}^{-1} \tag{2}$$

where K_{IC} denotes the fracture toughness [61, 63] (0.5784 MPa√m for the material), $L_{cr}= l_{max}/c$ (l_{max} is defined as the peak possible value for the length of the coalesced wing cracks, and 2b means the distance between the two flaws). In this paper, the initial flaw density of the prism containing four flaws is ε_0=0.03 ($\varepsilon_0=Nc^2/A$ denotes that N=4, A=0.2m × 0.3m and c=0.0212 m). Using Eq. (2) the compressive strength of the unit interlocking brick is calculated to be 6.43 MPa, which corresponds to 119.59 kN for this 1-block prism.

As illustrated in Eq. (2), the theoretical compressive strength for interlocking prism comprising of multiple bricks would be identical because the flaw density ε_0 is the same for one-block and multiple-block prisms. However, this may not necessarily be true because brick prisms comprising of more bricks have more interlocking joints, which could weaken the compressive load-carrying capacity. Laboratory test is conducted to validate the above theoretical derivation. Tests are extended from 1-block prism to 2-block and 4-block prisms in Section 3.

3. Experimental Investigation

Laboratory testing results are presented in this section. Firstly, the material properties for the interlocking bricks are quantified. Then, uniaxial compressive tests are carried out on 1-block interlocking brick prism to verify the above analytical solution. Tests are then extended to 2-block and 4-block prisms to further verify the accuracy and suitability of the above solution.

3.1 Material property test

To characterize the compressive properties of the brick material, uniaxial unconfined compressive tests are carried out using a SHIMADZU-50 machine. Three 50 mm diameter by

100 mm length specimens are core-drilled from the bricks and finely grinded on both ends (see Figure 3a). Strain gauges are glued on the specimens to measure the axial strain. Following ASTM C140 [64], unconfined uniaxial compressive test is conducted at a constant speed of 0.03 mm/s using displacement control method. Figure 3b) shows the measured compressive stress-strain curves, where the stress is defined as the measured axial force divided by the specimen cross-sectional area, and the strain is recorded using the strain gauges.

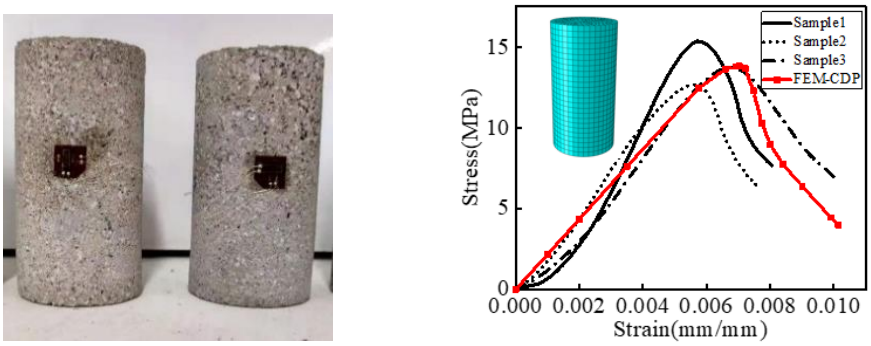

a) Core specimens b) Stress–strain curves

Figure 3. Material properties

3.2 Prism test

Brick prisms comprising of one block, two blocks and four blocks are tested under uniaxial compression. The prisms are built by stacking the blocks on top of each other without mortar. Brick prism compressive tests are conducted with reference to EN1052-1 [65]. It is worth noting that there is no testing or design standard available yet for interlocking brick.

SHIMADZU-300 Universal Testing System at Curtin University is used for the compressive test. A stiff steel plate (150 mm ×300 mm ×20 mm) is used to distribute the compressive load from the loading platen to the prisms. A constant loading rate of 0.03 mm/s is applied through the loading platen to the brick prism specimens. Two laser LVDTs (linear variable differential transducers) are installed at the two sides of the brick prisms to measure the compressive displacements of the prisms during testing. The averaged values measured from two laser LVDTs are taken as the compressive displacement. The compressive load is monitored by a load cell embedded in the loading machine. A typical prism set-up is shown in Figure 4 (2-block prism). Three specimens for each type of prisms are tested.

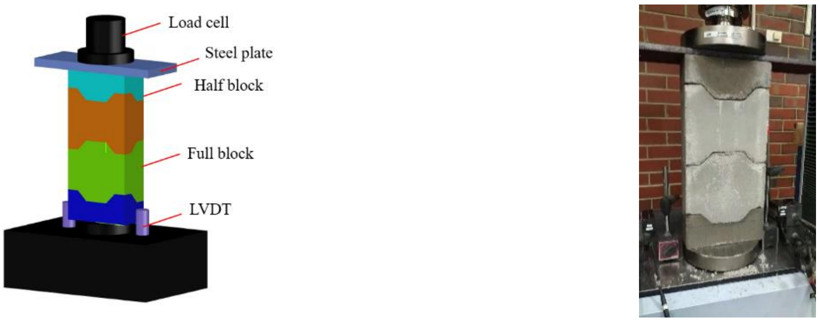

Figure 4. Compressive test setup for 2-block prism

3.2.1 Failure modes

Figure 5 shows the typical compressive failure process of the 1-block prism. The initial crack appears at the inner flaw tip of the concaved shear keys of the central brick at approximately 80% of its peak load, which propagates downwards with the increase in compressive load. This is consistent with the theoretical assumption and formation of wing crack (Figure 2) in Section 2. The crack develops into crack coalescence till the peak load is reached. Then more cracks appear both in the central brick of the top convex interlocking key. The cracks continue to develop until the applied load is stopped.

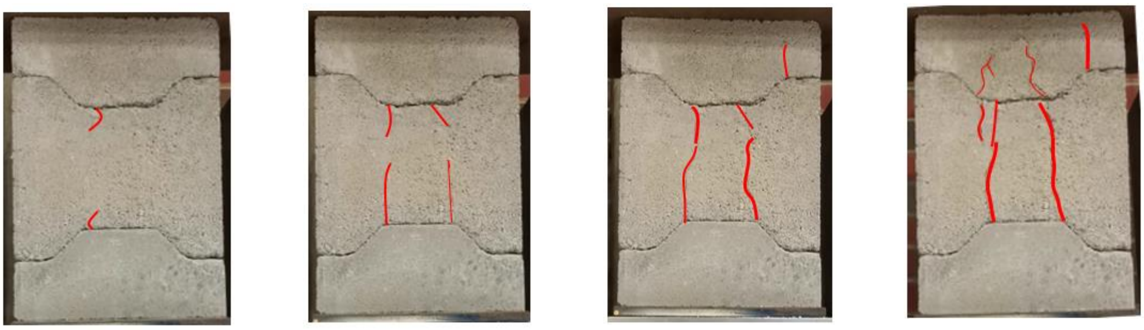

(i) Stage 1 (ii) Stage 2 (iii) Stage 3 (iv) Stage 4

Figure 5. Typical damage-to-failure progress of 1-block prism: (i) tensile wing cracks initiate; (ii) cracks extend from key and propagate downwards; (iii) crack coalescence; (iv) more cracks occure near the contact region

3.2.2 Compressive load-carrying capacity

Figure 6 summarizes the ultimate compressive load-carrying capacities of the 1-block, 2-block and 4-block prisms. The theoretical predictions are also included for comparison. An averaged compressive capacity of 128.3 kN is measured for the 1-block prism, which is very close to the theoretical prediction of 119.59 kN. It is apparent that the compressive capacity of the interlocking brick prism decreases with the increased number of blocks, indicating the compressive strength of interlocking blocks is influenced by the number of blocks. For example, an averaged compressive capacity of the 2-block prisms is 108.5 kN, and that of the 4-block prisms is 102.9 kN. This is because the increased number of interlocking joints introduces more weak sections for the prisms. The theoretical prediction is based on the analysis of 1-block prism, therefore could not take this into consideration, hence results in a +10.22% and +16.22% overestimation of loading capacities of the 2-block and 4-block prisms, respectively. Considering more bricks in the theoretical derivation is not straightforward because of more weak sections and flaws. In the subsequent sections, numerical models of prisms with different number of bricks are developed, and numerical analyses are carried out to investigate the influences of the number of bricks on the load-carrying capacities of interlocking masonry blocks.

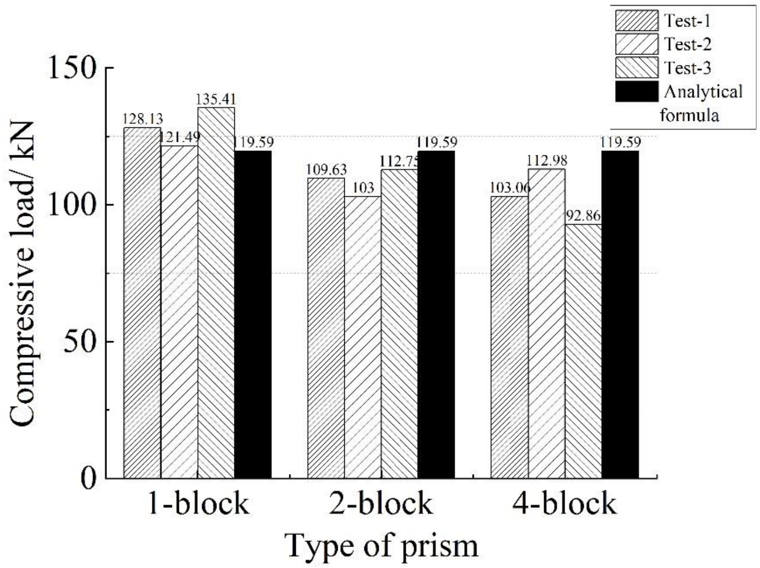

Figure 6. Comparison of experimental and analytical compressive loads

4. Numerical Modelling

To better understand the behaviour of interlocking bricks and facilitate further parametric study, detailed three-dimensional numerical models of interlocking brick prisms are generated. The models are used to simulate the laboratory tests and the results are compared with those recorded in the tests to verify the accuracy of the numerical model. The material model is firstly described, followed by the details of the numerical models of the interlocking prisms. As discussed above, contacts between interlocking bricks affect the performances of mortar-less masonry blocks made of interlocking bricks, which are not straightforward to be accurately modelled. To investigate the modelling accuracy and efficiency, three different contact methods are used and compared. The numerical results are presented and compared with the laboratory testing results.

4.1 Material model

The commercial software ABAQUS [66] is used in this study. To simulate the nonlinear behaviour and damage of the interlocking prisms, the concrete damage plasticity (CDP) model proposed by Lubliner et al. [67] to predict the behaviour of concrete and other brittle materials is used. Crushing in compression or cracks in tension from micro- to macro-levels can both be modelled. CDP model assumes that the uniaxial compressive and tensile failures of the material are characterized by damaged plasticity (see Figure 7). Material hardening and softening behaviour can also be incorporated by this model.

The compressive strength, tensile strength, initial Young's modulus and the relationship between stress and strain are defined. The compressive strength of the material is obtained from the material tests presented above. The initial Young's modulus is taken as a secant modulus and is measured from the slope at a stress extent equal to 40% of the ultimate compressive strength. Poisson's ratio is determined at the same extent of the stress, which is obtained by the ratio of the transversal strain over the longitudinal strain. The material properties adopted for the interlocking blocks are given in Table 1, where E_0 is the initial Young's modulus; v is the Poisson's ratio; and f_t is the tensile strength. The tensile strength is obtained as f_t=0.1f_c, which is a relation often used for concrete material [68, 69].

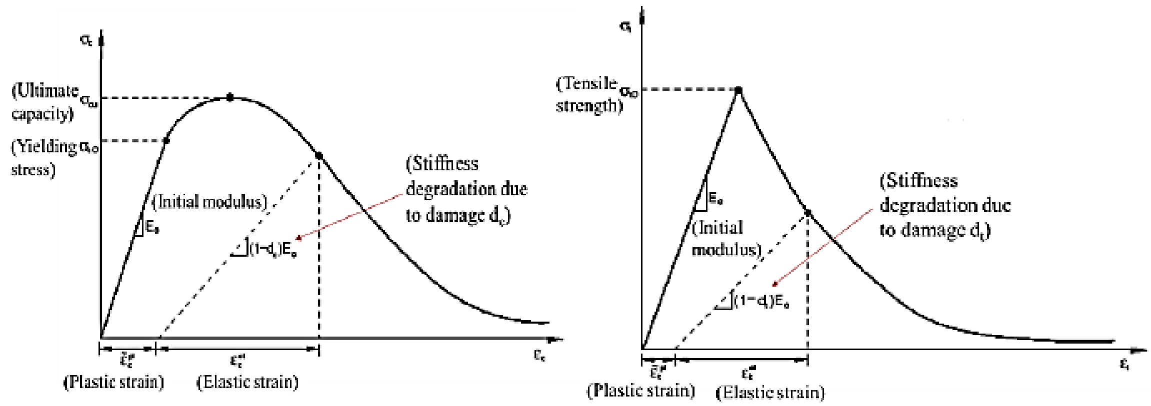

a) Compressive behaviour b) Tensile behaviour

Figure 7. Illustration of concrete damage plasticity model [68]

Table 1. Brick material properties

Mass density (kg/m^3)	Elasticity		Plasticity				
	Initial Young's modulus, E_0 (MPa)	Poisson's ratio υ	Dilatation angle ψ (°)	Eccentricity	Biaxial stress ratio f_{bo}/f_{co}	K	Viscosity Parameter
2565	2184.58	0.2	35	0.1	1.16	0.65	5E-5

Note: *K* is the ratio between the second stress invariant on the tensile meridian and compressive meridian at initial yield.

Table 2. Material constants for the CDP model in Abaqus

Compressive behaviour		Tensile behaviour	
Yield stress	Inelastic strain	Yield stress	Cracking strain

(MPa)		(MPa)	
12.74	0	1.38	0
13.78	0.0003	1.24	0.0012
13.05	0.0015	1.19	0.0014
10.81	0.0034	1.14	0.0016
8.64	0.0052	1.09	0.0018
7.10	0.0067	0.80	0.0030
1	0.0200	0.56	0.0040

To evaluate the accuracy of the model and material parameters, uniaxial compression tests on the 50 mm length by 100 mm diameter core specimen is numerically modelled. As shown in Figure 3b), the column is meshed with solid element of size 4 mm × 4 mm× 4 mm in longitudinal, transverse and thickness direction respectively, and the material parameters are presented in Table 2. As shown in Figure *3*b, the stress-strain curve from the numerical results (as highlighted in the red curve – FEM-CDP) agrees reasonably well with the laboratory testing results.

4.2 Model details

Three-dimensional models of the interlocking brick prisms with solid elements are generated to model the interlocking block prisms. The C3D8R type element (3D 8-node linear with reduced integration) is selected which is an eight-node solid element with three translational degrees of freedom per node. The reduced integration is calculated by the incorporation of the lower-order rigidity of the unit, while the distributed loads and the mass matrix are determined by full integration. This element can be used to improve the calculation efficiency, and to obtain more accurate stress fields and displacements. For the interlocking brick prism, the axial and hoziontal degrees of freedom at the base are restrained, whereas the nodes of the top block are restrained to prevent lateral movements and vertical movement is allowed. Displacement control loading method is used, which follows the loading method used in the tests. Nonlinear analysis is used in the numerical modelling.

4.3 Convergence study

Mesh convergence study is conducted by gradually reducing the mesh size from 56 mm to 3.5 mm. As shown in Table 3, further reducing mesh size from 7 mm to 3.5 mm yields minor changes in the computed maximum peak compressive force but the computational time increases substantially. Therefore, 7 mm mesh size is adopted for the numerical model in this study.

Table 3. Mesh size convergence study

Mesh size (mm × mm × mm)	Peak compressive force (kN)

56 × 56×56	177.82
28 × 28×28	152.27
14 × 14×14	138.81
7 × 7×7	118.29
3.5 × 3.5×3.5	112.46

4.4 Contact algorithm

Three different modelling methods, i.e. perfect contact, imperfect contact and cohesive element contact are considered herein to simulate the contact behaviour at the interlocking brick joints. The perfect contact is the fundamental method used by most engineers, which assumes the brick surfaces are smooth and in perfect contact condition with adjacent bricks. The imperfect contact method considers predefined gaps at the joint to model the imperfect surface condition of the brick. The cohesive contact method employs a cohesive element to deal with the non-linear behaviour at the joint. These three different types of contact model are detailed below:

4.4.1 Perfect contact

Perfect contact assumes the two surfaces of adjacent blocks match perfectly and ignore surface roughness condition. A contact pair is composed of the neighbouring contact surfaces, which can prevent penetration between the interlocking bricks. It provides a method for ensuring an appropriate transformation of forces between two interlocking bricks on the basis of tangential and normal contact behaviour. This study takes into account of both the normal contact behaviour, which dominates the penetration between the two interlocking bricks, and the tangential contact behaviour used to model sliding between adjacent bricks depending on the friction coefficient [70].

For tangential behaviour, the Mohr-Coulomb criterion is applied into the contact model. $\tau_{\mathrm{lim}}=\mu_{\sigma}+c_{\mathrm{c}}$, where τ_{lim} denotes the limit for shear stress at which sliding starts, μ denotes the coefficient of friction, σ denotes the pressure of normal contact, and c_{c} denotes the cohesion of contact. There is no relative sliding between the contact surfaces before the tangential force reaches the critical shear stress, while the contact surface slides when the shear stress exceeds τ_{lim}. In this study, the friction coefficient is set to be 0.3 between the interlocking blocks and 0.15 between blocks and steel plates [69, 71], and for dry joints, contact cohesion is negligible (c_{c}=0) [72].

4.4.2 Imperfect contact

As discussed in the introduction, due to unavoidable manufacture error/tolerance and surface roughness, imperfect contact with small invisible gaps at the interfaces occurs most of the time between bricks. Rough surfaces involve lots of asperities (or valleys and peaks). For modelling the uneven surface roughness, the imperfection distributions existing in the interlocking blocks are firstly examined and quantified experimentally.

Experimental measurements of surface unevenness

Fifteen interlocking bricks are selected randomly from the same batch of bricks in this study. The experimental setup is illustrated in Figure 8a). The specimen is mounted on a flat table which provides a flat reference surface for measurement of imperfections. A surface height dial indicator is used to measure the absolute height of the brick surface along the key joint at 0.25 mm intervals along the section of the brick to map out the profile of the cross-section. As shown in Figure 8b), the mortises are surface S1, S5 and S6, and tenons are surface S2, S3 and S4. A total of 60 tenons and 30 mortises are measured. Figure 9 shows the surface unevenness measurement results. With respect to the lowest point of each surface, the asperity height varies from 0 mm to 0.2 mm for the mortise (S1,5,6), while tenons (S2,3,4) are rougher with the roughness amplitude varying from 0 mm to 0.3 mm with over 55% frequency of 0.1 mm. For a typical joint comprising of two interlocking blocks, to obtain the average gap length between the mortise and tenon, from the baseline of a brick (Figure 8b), the absolute roughness amplitudes from all measured points on each surface are averaged to obtain the average roughness amplitude of the surface. The average relative gap width Gap_2 between S2 and S5 can then be calculated as $Gap_2=h_5-h_2$, in which h_5 and h_2 are the average roughness amplitude of S5 and S2, respectively. Similarly, the average gap width between S1 and S4, and S6 and S3 can be calculated as $Gap_1=h_4-h_1$ and $Gap_3=h_6-h_3$, respectively. As shown in Figure 9, compared to the Gap_1 and Gap_3 of the tenons, the Gap_2 could be ignored. Therefore, the S1 and S4 contact is assumed as perfect contact, hence it is idealized that there is no pointwise contact due to uneven surfaces. As illustrated in Figure 8c), once the joint is under compression, the compressive force will push the central gap between S1 and S4 to close, but leave a gap between S2 and S5, as well as S3 and S6. Therefore, an idealized imperfect contact model is generated with the central contact surfaces being fully closed but the two adjacent contact surfaces have a uniform gap of width 0.1 mm. The uniform gap width of 0.1 mm is an assumed value based on the measured roughness amplitude shown in Figure 9. Because the roughness profile on each brick surface is basically random, it is not possible to exactly model them in the numerical model, therefore simplification is made. In this study the gap width is based on the average roughness amplitudes measured from the brick surfaces. This simplification allows engineering assessment of the influence of surface unevenness in numerical simulations.

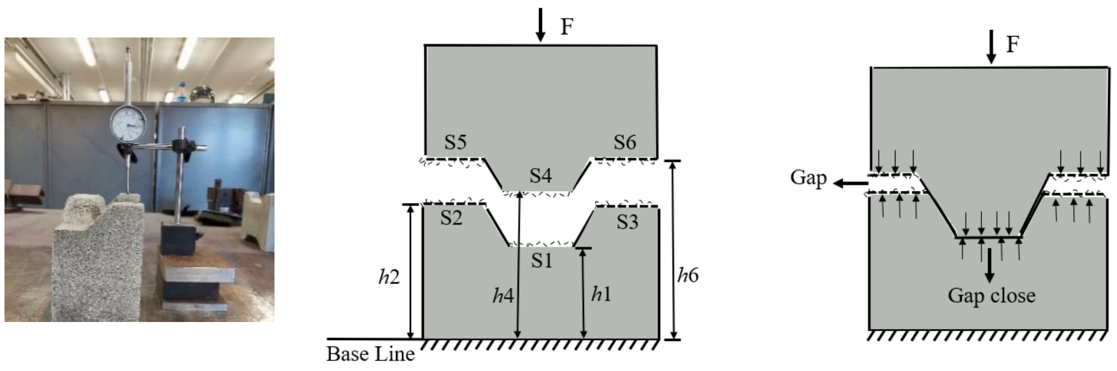

a) Test setup b) Illustration of gap measurement method c) Imperfect contact model

Figure 8. Surface roughness examination and modelling

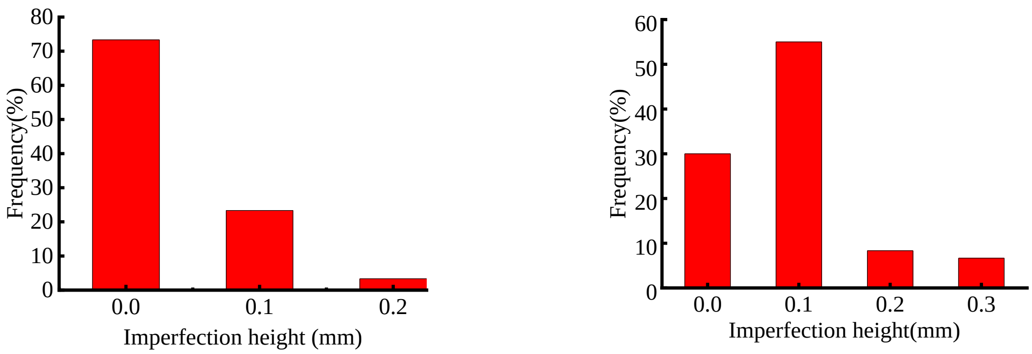

a) Mortise b) Tenons

Figure 9. Results of the roughness surface

4.4.3 Cohesive contact

Cohesive element can be introduced to model the complex contact behaviour between two adjacent surfaces, whose stiffness could degrade after the pre-defined threshold criteria due to the shear and tensile deformations [46]. It enables the study of the cohesive behaviour and damage for the interlocking bricks to consider the surface unevenness and friction interaction.

In this study, a cohesive element of zero-thickness is used to model the interaction between two interlocking bricks. The constitutive model for the cohesive element employs the traction-separation law in ABAQUS. It assumes an initially linear elastic behaviour at the interface. As the compressive load increases and reaches the pre-defined stress, interface evolution and damages are triggered. Then, the friction model is activated which attributes to the shear stress [44]. The friction behaviour is modelled based on the Mohr-Coulomb failure criterion. The compressive stiffness is taken as 10 times that of the Young's modulus of the interlocking brick following reference [2]. The in-plane and out-of-the plane shear stiffnesses are taken as 0 since only the compression behaviour is considered. The maximum nominal stress for damage propagation is used here. The selected properties of interfaces available in the numerical simulation are tabulated in Table 4.

Table 4. Properties of interface

Interface Properties	Interface behaviour
Normal stiffness (N/mm)	21800
Shear stiffness (N/mm)	0
The coefficient of friction	0.3
Maximum tensile stress (MPa) [44]	0.68
Maximum shear stress (MPa)	0

5. Results and Analysis

The laboratory testing results and numerical modelling results are presented in this section. Compressive force versus axial displacement curves, brick prism damage and failure modes, and ultimate compressive load-carrying capacity are compared and examined.

5.1 Force-displacement curves

Figure 10 shows the axial load-displacement curves for the 1-block, 2-block and 4-block prisms under compression. As shown, for the 1-block prism, the load increases slowly to about 20 kN at about 1.3 mm axial displacement, which is because of seating effect [69] that the gaps between the bricks close. As joints gradually close, the slope of the curve increases, and the compressive load also quickly rises almost linearly with displacement till the ultimate load at about 128 kN, after which it begins to drop, indicating the damage of the block. Among the three tested 1-block specimens, differences can be found in the force-displacement relations, which are because of the inherent variability at the interface of dry-stacking bed joints block and the variations between units in material properties [69]. Similar behaviour can be observed for the 2-block and 4-block prisms that the initial displacement for seating effect increases with the increase in the number of blocks hence the number of gaps. This is because asperity interactions at prism interfaces increase with the increase in the number of blocks. More asperities could be worn when more blocks are under compression. For the 4-block prisms, peak loads of about 100 kN are achieved at around 4mm displacement. Larger vertical displacements are observed on the 4-block prisms as compared to those of the 1-block and 2-block prisms. After reaching the peak load, the load quickly decreases with further increased displacement.

Figure 10 compares the load-displacement curves of the numerical models using the above-mentioned three contact methods. Since the numerical model could not accurately represent the seating effect, their axial force-displacement curves are aligned with the experimental load-displacement curves after the initial gap is believed to be closed. It can be found that the numerical models with perfect and imperfect contacts could closely represent the stiffness of load-displacement curves after the gaps at the joints are fully closed as well as the ultimate compressive load. For example, for 1-block prisms the numerical load-displacement curves match the test curves relatively well if they are shifted by 1.3 mm, i.e., the initial seating displacement of the tested 1-block specimen. The compressive load increases almost linearly with displacement till about 80% of the ultimate strength, and then the stiffness begins to degrade indicating the damage of the brick. The predicted ultimate compressive loads with the three contact models, namely perfect contact model, imperfect contact model and cohesive model are 118.29 kN, 114.93 kN and 97.19 kN, respectively. The corresponding stiffnesses are 99.98 N/mm, 95.97 N/mm and 88.11 N/mm. As shown in Figure 10b) and 10c), as the number of brick increases, more apparent seating effect can be observed. The numerically modelled load-displacement curves for the 2-block and 4-block prisms are shifted by 1.5 mm and 2 mm respectively to align with the experimental curves. For the perfect and imperfect contact models, the load increases quickly to about 110 kN at about 3 mm axial displacement for the 2-block prism and about 105 kN at about 4 mm axial displacement for the 4-block prism. As shown, for the 2-block and 4-block prisms, the perfect contact model predicts a compressive stiffness of 71.18 N/mm and 44.71 N/mm, and the corresponding values from the imperfect contact model are 65.73 N/mm and 41.71 N/mm, respectively. The cohesive contact model gives the lowest compressive stiffnesses of 63.71 N/mm, 40.49 N/mm with the ultimate compression capacity of 93.96 kN and 91.67 kN, respectively. As shown in the above figures, the numerical models can reasonably well predict the stiffness and ultimate load-bearing capacity of the masonry blocks, although they cannot simulate the process of asperities compaction from the initial surface contact to complete contact. Furthermore, the post-peak behaviour of the interlocking prisms cannot be fully modelled with the numerical methods which drops quicker and has less residual capacity in comparison to the laboratory test results. This is probably because of the material model used. Nevertheless, for design purpose since only compressive stiffness and ultimate compressive capacity are of primary interests, further modification of the numerical model to achieve better post peak behaviour is not conducted in this paper.

Through the above comparisons it can be found that the perfect contact model omits the rough surface effect in terms of varying peak height of the asperities. Slightly larger stiffness and ultimate load are therefore predicted by the perfect contact model as compared to the imperfect contact model. It is clear from Figure 10 that the cohesive contact model considerably underestimates the stiffness and the ultimate strength of the interlocking prisms, which is probably because the stiffness of the cohesive element is underestimated in the numerical model in comparison to that of the actual contact surface. Therefore, the numerical models with perfect and imperfect contact predict reasonably good result for both the compressive stiffness and ultimate load-carrying capacity of the interlocking brick prisms. Further studies with advanced numerical modelling technique to describe the roughness and imperfect contact surface so as to model the seating effect is under development.

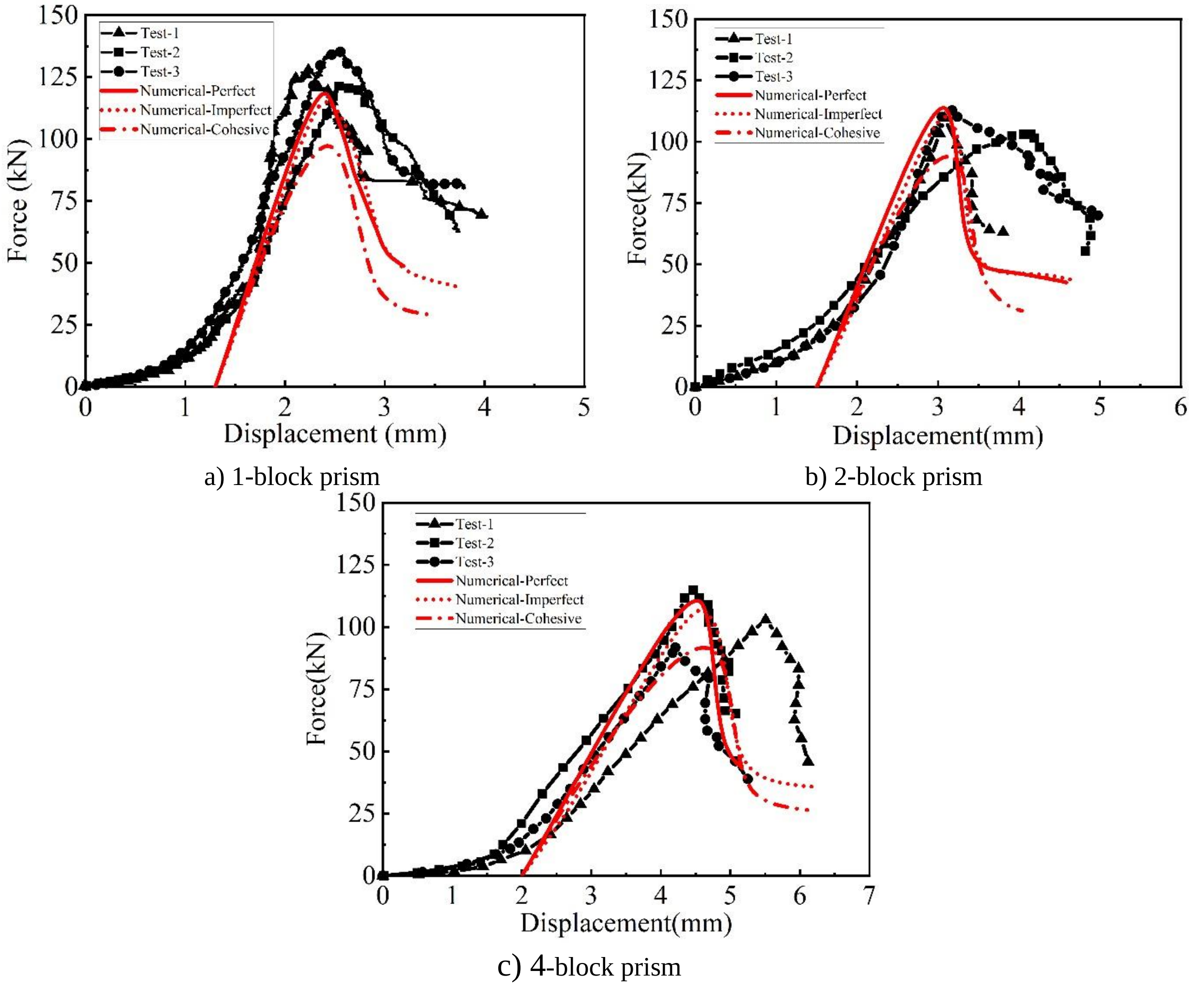

a) 1-block prism
b) 2-block prism
c) 4-block prism

Figure 10. Load-displacement curves from laboratory test and numerical simulation

5.2 Crack propagation

Figure 11 illustrates the crack propagation processes of the prisms in stages with respects to the load-displacement curves. Tensile wing cracks can be found near the tenon and mortise, which initiate from flaw tips and extend in a steady pattern towards the direction of maximum compression [73]. It can be observed that for the 1-block prism wing cracks initiate from around the corner of the shear tenon when the applied compressive load is about 105 kN, and extend slowly along the compressive loading direction until the ultimate compressive force of 115 kN is reached. Two thorough vertical cracks are developed. With further increased vertical displacement, the cracks further extend vertically and interact with neighbouring microcracks, which lead to crack coalescences as well as ultimate failure of the prism [59, 74]. In the numerical model, the initiation and growth of crack are both controlled by the stress field near the existing interlocking key. The numerical simulation agrees with experimental observations in that cracks initiate at about 80% of the peak load around the shear tenon, and extend along the vertical direction and result in the crack coalescence till the peak load is reached. Then these cracks grow wider with the increased load. Similarly, for the 2-block prisms, from both the numerical simulations and experimental observations it can be found that crack initiation occurs at 80% of the peak load and crack coalescence at the peak load is firstly presented on the concaved shear keys. With the increase in the applied displacement and load, a growing wing crack is developed at the outer tip in the middle of the bridge area [61] of the convex block, which is associated with wider and more cracks. The growth of cracks at the inner tips is faster than those shown at the outer tips, which agrees with that in the experimental observation. This is due to the higher stress concentration near the inner joint tip which enables the crack to propagate further. For the 4-block prisms, similar crack initiation and development can be observed. For multi-block prisms when the maximum compressive load is reached (corresponding to the second point in the figure), crack coalescence initiation occurs in the inner tip of the concaved interlocking key, and then these cracks propagate up and down forming a thoroughly penetrated crack. The crack pattern agrees well between numerical modelling and experimental observation.

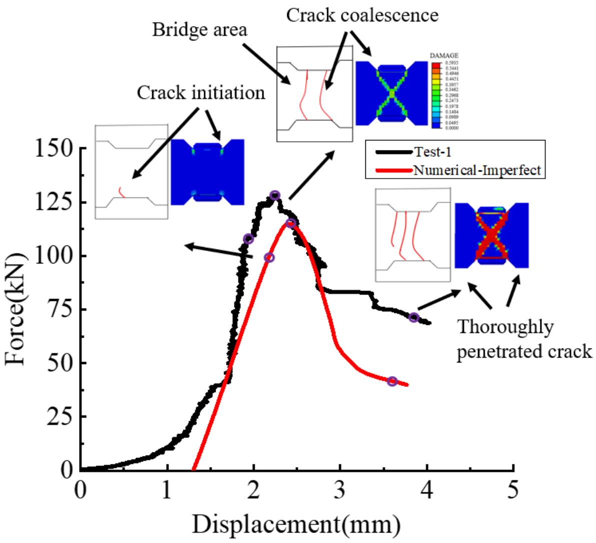

a) 1-block prism

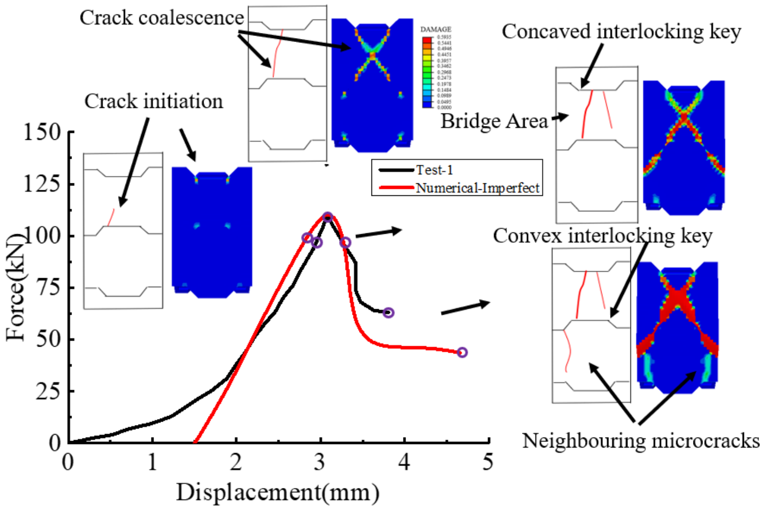

b) 2-block prism

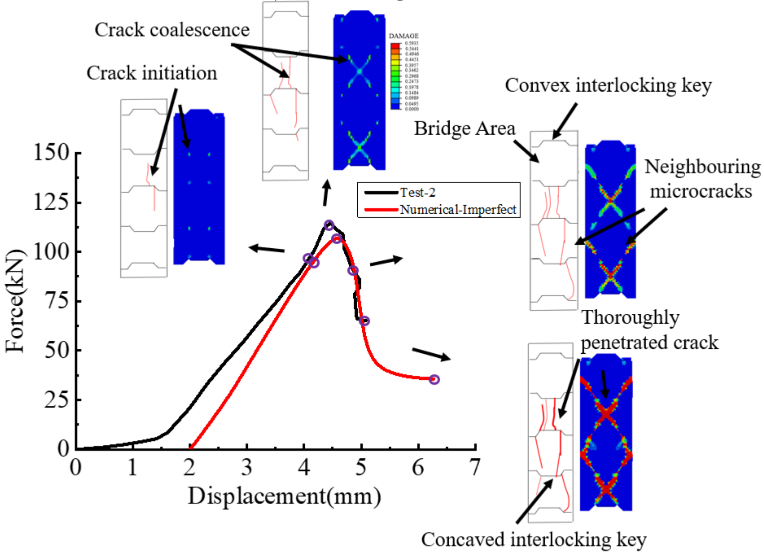

c) 4-block prism

Figure 11. Prism crack initiation and development in the experiments and numerical simulations

5.3 Failure modes

Figure 12 summarizes and compares the damage modes of the interlocking prisms from the laboratory tests and numerical modelling. Both the laboratory test and the numerical model show wing cracks occur around the shear keys. For the perfect contact model, cracks at the unit interface propagate up and down from the flaw tips at an angle of 45°, exhibiting an X shape failure mode across the prism. The numerical models with cohesive contact model predict inclined cracks through the full block, which differs from the test observations. Through the comparisons, it can be found that the predictions from imperfect contact model most closely match the observed damages in the test among the three models, although some deviations are obvious. For example, the damages predicted by the numerical model is basically symmetric, whereas they are not necessarily symmetric in the tests. These differences can be attributed to the non-perfect contact conditions between adjacent interlocking bricks, and also possibly non-uniform material properties of the brick. Nonetheless, it can be concluded that the simplified imperfect model yields the closest predictions of the failure pattern of the interlocking brick prisms under compression.

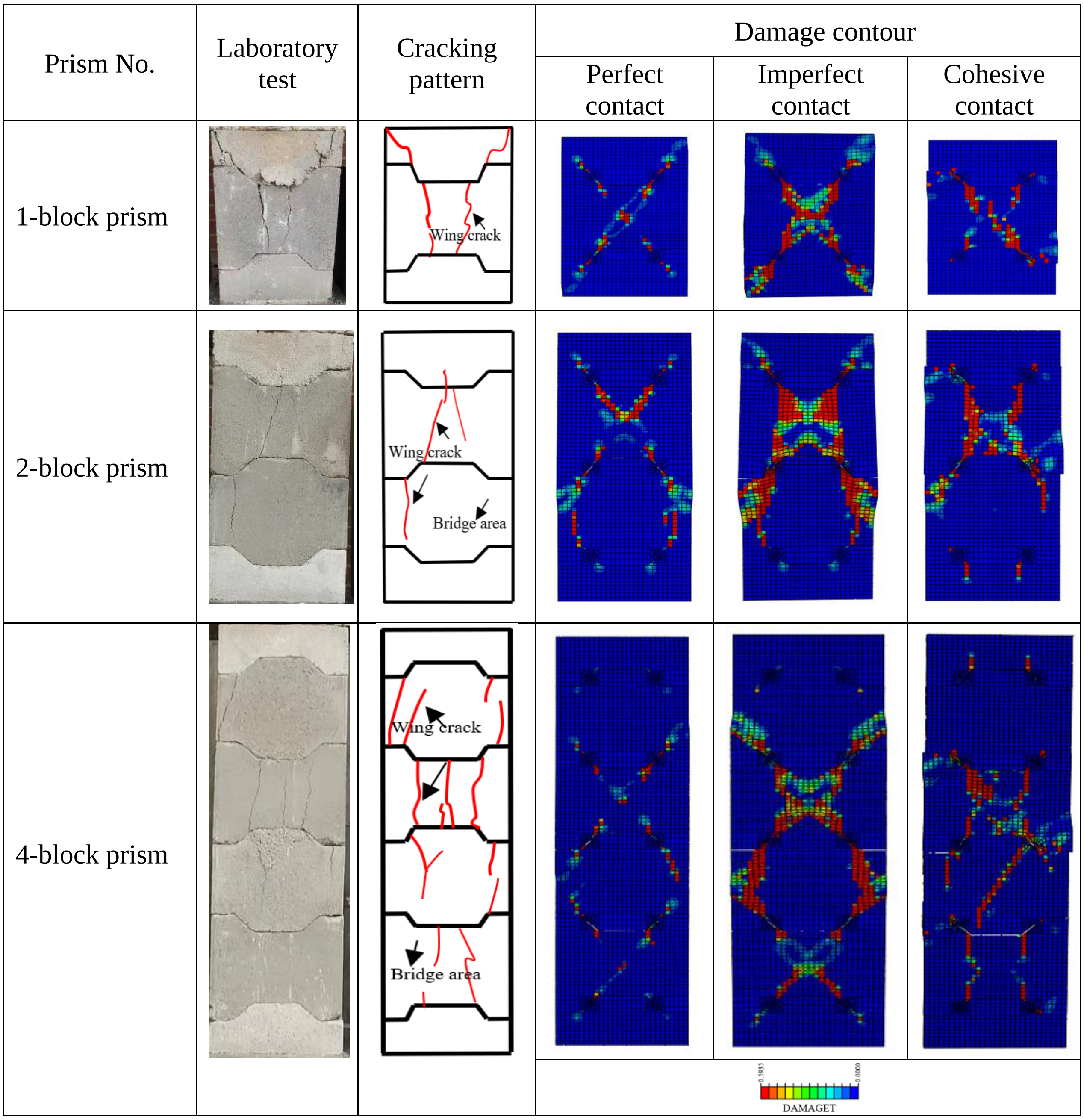

Figure 12. Comparison of prism damage modes

The above results and analyses show the compressive behavior of interlocking brick prism is strongly influenced by the number of blocks. The compressive strength decreases with more blocks in prisms. Wing cracks are initiated from the protruded key tenon and mortise which is similar to the assumption of fracture mechanism theory. The developed numerical models could reasonably predict the behavior of the interlocking brick prisms. The imperfect contact modeling method gives the closest prediction.

6. Parametric Study

Parametric study is carried out in this section to examine the influences of the number of blocks, the level of brick surface roughness amplitude, and material strength on the compressive load-carrying capacity of the interlocking brick prism. An empirical formula is derived based on the numerical modeling results, experimental results, and analytical solution to predict the compressive load-carrying capacity of the interlocking brick prism. A semi-empirical method is also generated to estimate the compressive stiffness of the interlocking brick prism.

6.1 Effect of block number

A series of numerical simulations are carried out with gradually increased number of blocks for the prism until the ultimate compressive load converges. In the meanwhile, roughness amplitude due to brick surface imperfection and unevenness is assumed to be 0.1 mm, and the material compressive strength is 13.78 MPa in the numerical modellings. The cross-section area, brick size and interlocking key dimension are kept the same.

Figure 13 shows the results combining the prism ultimate compressive load with the number of blocks. It can be observed that as expected the influence of the number of blocks on the compressive load-carrying capacity of prisms is significant. For example, the equivalent compressive strength drops quickly from 6.18 MPa for 1-block prism to 5.93 MPa for 2-block prism, and further to 5.75 MPa for 4-block prism. Nevertheless, as the number of bricks in the prism increases, the decreasing speed also gradually reduces. The compressive strength reduces from 5.59 MPa for 8-block prism to about 5.52 MPa for 10-block prism (-1.3%), which further reduces to about 5.51 MPa for 12-block prism, indicating an ignorable -0.2% decrease.

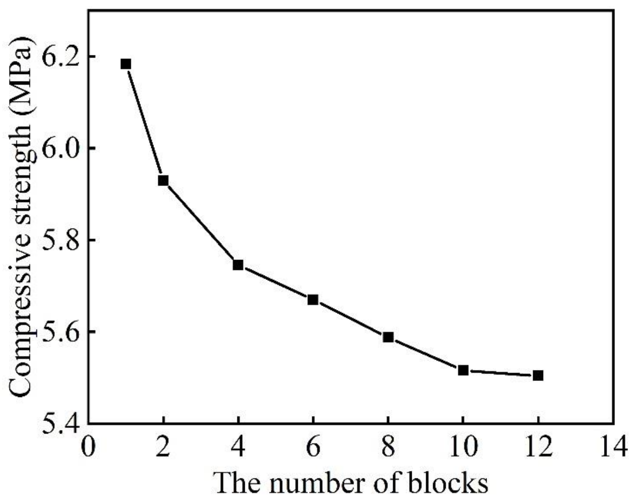

Figure 13. Ultimate compressive strength for interlocking brick prisms with different numbers of brick

6.2 Effect of brick surface roughness amplitude

As demonstrated above in the laboratory test and numerical simulation, since joint imperfection due to brick manufacturing error/tolerance and surface unevenness could strongly influence the interlocking prism compressive strength, the interlocking bricks with surface roughness amplitude varying from 0 mm to 0.25 mm with a 0.05 mm increment are numerically modeled to quantify its influence on prism compressive strength. The cross-section area, brick size and interlocking key dimension are kept the same. The material compressive strength is also 13.78 MPa in the numerical simulations.

Figure 14 shows the results combining the prism ultimate compressive load with imperfection roughness amplitude and the number of blocks in the prisms. It can be observed that the compressive capacity of the interlocking brick prism with the same number of bricks decreases with the increased roughness amplitude. For example, for the 6-block model with roughness amplitude of 0.1 mm and 0.25 mm, the ultimate capacity decreases to approximately 5.09 MPa from 5.67 MPa; for the 12-block prism, the ultimate capacity decreases from 5.51 MPa when the roughness amplitude is 0.1 mm to 4.87 MPa when the roughness amplitude is 0.25 mm. These results indicate that the roughness amplitude also has strong influence on the prism compressive capacity.

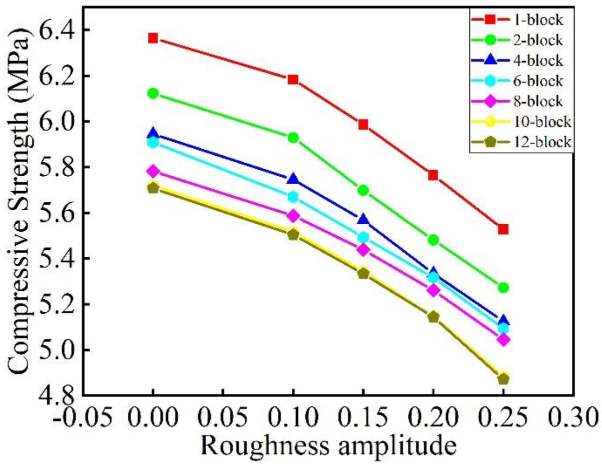

Figure 14. Ultimate compressive strength for interlocking brick prisms with different roughness amplitudes

6.3 Effect of material strength

To examine the influence of material strength (f_{brick}) on the compressive strength of the interlocking prism, numerical simulation is conducted with f_{brick}varying between 13.8 MPa and 30 MPa with around 5 MPa increment. The Young's modulus is taken as 160 times the compressive strength of the material, and the material tensile strength is $0.1f_{brick}$ [69]. The roughness amplitude is assumed to be 0.1 mm.

Figure 15 presents the compressive strength of the prisms of different number of blocks with respect to the material compressive strength. For instance, for the 10-block model the ultimate compressive strength increases from approximately 5.52 MPa to 9.30 MPa when the material strength increases from 13.8 MPa to 30 MPa. As expected, the compressive strength of interlocking brick prisms is strongly influenced by the material strength, and the prism loading capacity shows a near-linear relation with the material compressive strength. Moreover, the ratio of the prism strength to the material strength is approximately 0.23, and is dependent on other parameters such as the brick surface roughness amplitude and the number of bricks as discussed above. However, the influence of these parameters is not as significant as the material strength.

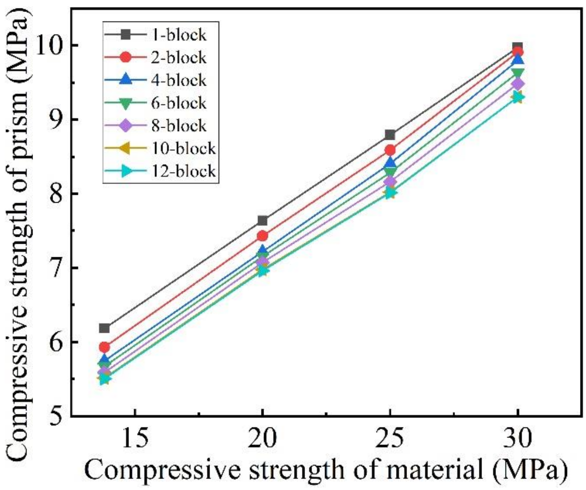

Figure 15. Ultimate compressive strength for interlocking brick prisms with different material strength

6.4 Modified design formula for compressive strength

To account for the influence of the number of blocks, and the brick surface roughness amplitude as demonstrated above in engineering analysis and design, modification to the analytical solution of Eq. (2) is made by introducing to correction factors, i.e. $f(n_{block})$ and $g(h_{imp})$. In addition, to account for the variation of material strength, another term $\mu(f_{brick})$ is also introduced. The compressive strength of an interlocking brick prism, $\sigma_{n,h}$, could be expressed using the following equation

$$\sigma_{n,h} = \sigma_1^{max} * f(n_{block}) * g(h_{imp}) * \mu(f_{brick}) \tag{3}$$

where σ_1^{max} is the unit block compressive strength of the analytical solution given in Eq. (2).

Regression analysis on the laboratory testing and numerical modeling results is conducted to derive the above modification components in the proposed formula. Regression models are considered to achieve a best-fitted formula. The adequacy of regression models is evaluated with the coefficients of determination (R^2). The Eq. (4) with high R^2 of 94.7% is therefore chosen, which reflects the prism strength is positively proportioned to material strength, and negatively related to the number of bricks and roughness amplitude.

$$\sigma = \sigma_1^{max} * (0.199 f_{brick} + 2.238) * \left(0.133 + \frac{1}{1.933 * n_{block} + 22.076}\right) * \frac{1}{0.784 h_{imp} + 0.855} \tag{4}$$

To evaluate the accuracy of the proposed formula, Figure 16a) compares the formula predicted prism strength with those obtained from tests and numerical calculations. It can be found that the prediction using the proposed formula could closely predict those from the numerical simulations and experimental tests with the ratio of $\sigma_{test}/\sigma_{pred.}$ consistently distributing around the surface of 1.0.

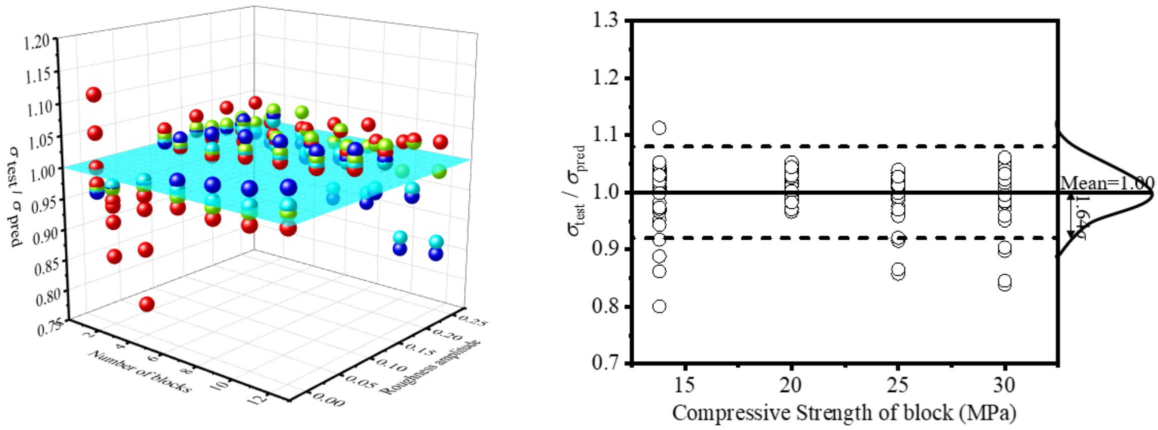

a) b)

Figure 16. a) Comparison of the prism compressive strength estimated from the proposed formula and the test and the numerical results; b) predictions of different compressive strengths of interlocking imperfection prisms

For engineering design purpose, to account for uncertainties such as material strength, the above proposed prediction formula is further integrated with a safety margin by setting a confidence limit. Following CSA-S304.1 [75], the specified compressive strength for the interlocking brick prism can be determined with 95% confidence. Assuming the ratio of $\sigma_{test}/\sigma_{pred.}$ to follow normal distribution, the 95% confidence can be determined by subtracting 1.64 times the standard deviation from the arithmetic mean. Therefore, the confidence lower limit for a standard deviation of 0.047 and a mean of 1.00 can be estimated to be 0.92 (as shown in Figure 16b). Therefore, Eq. (5) can be presented appropriately for engineering assessment though re-evaluating as:

$$\sigma = 0.92\ \sigma_1^{max} * (0.199 f_{brick} + 2.238) * \left(0.133 + \frac{1}{1.933 * n_{block} + 22.076}\right) * \frac{1}{0.784 h_{imp} + 0.855} \quad (5)$$

6.5 Semi-empirical method for prism compressive stiffness

A semi-empirical analysis method is proposed herein for simplified design purpose of interlocking prisms under uniaxial compression loads. A homogeneous prism is derived with an equivalent axial stiffness to predict the compressive properties for prisms comprised of different numbers of interlocking bricks.

a) Interlocking prism b) Equivalent model

Figure 17. the equivalent vertical stiffness of the interlocking prism

As demonstrated in Figure 17a), an interlocking brick prism with n pieces of bricks can be represented by a series of springs, i.e. K^{B} and K^{C} for the block stiffness and the interlocking contact stiffness, respectively. The equivalent spring stiffness K^{n} for a homogenous model (Figure 17b) can be written in the following forms:

$$1/K^{n} = \mathrm{n}/\,K^{B} + (\mathrm{n}+1)/K^{C} \tag{6}$$

For each block, its stiffness K^{B} can be calculated by

$$K^{B} = \frac{E_{mat}A_{block}}{L_{block}} \tag{7}$$

where E_{mat} is the Young's modulus of the material, A_{block} is the cross-sectional area of the brick, and L_{block} is the height of the brick. By using material constants and brick dimension, K^{B} is 338.37 kN/mm.

The equivalent axial stiffness of n-block prism K^{n} can also be expressed as

$$K^{n} = \frac{EA}{L} = \frac{\int_{x} F(x)dx}{\Delta l_{n} \times L_{n}} \tag{8}$$

where F is the peak compressive load, Δl_n is the corresponding axial displacement, and L_n is the height of the prism. The equivalent stiffness of 1-block prisms can be calculated with the laboratory testing data. And Eq. (8) is applied to the case of 1-block prism, the stiffness of contact surface K^{C} can be written by

$$K^{C} = \frac{2K^{1} \times K^{B}}{K^{B} - 2K^{1}} \tag{9}$$

So it can be calculated that K^{C} is 263.28 N/mm. With the above-derived K^{B} and K^{C}, the equivalent axial stiffness of the interlocking brick prism comprising of n-block can be easily estimated. Figure 18 presents the experimental tested prism stiffness and the estimated prism stiffness using the semi-analytical approach. It shows the equivalent stiffnesses predicted by Eq. (6) and those from the experiments agree reasonably well.

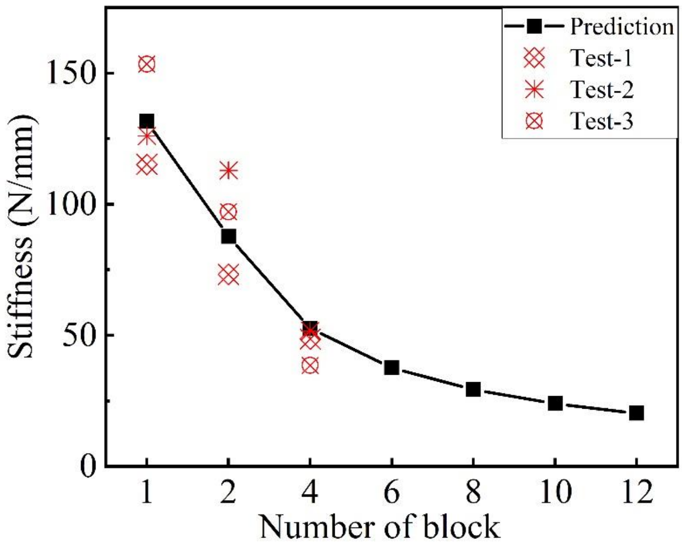

Figure 18. Equivalent compressive stiffness of interlocking brick prisms

7. Conclusion

This paper presents analytical analysis, laboratory testing and numerical modelling to investigate the compressive properties of interlocking brick prisms. The damage and failure modes of dry-stacking interlocking brick prisms are studied. Detailed numerical models of interlocking brick prisms are generated using different contact modelling methods, which are validated and verified with the laboratory tests. Parameter study is carried out to quantify the influences of the number of blocks, joint roughness amplitude due to brick surface unevenness, and brick material strength on the compressive load-carrying capacity. Combining the numerical simulation and testing results, an analytical prediction formula is derived to predict the compressive strength of interlocking brick prisms. A semi-empirical approach is also developed to estimate the compressive stiffness of interlocking brick prisms. The following conclusions are drawn from this study:

1. Fracture mechanism based analytical solution could closely predict the compressive strength of unit interlocking brick. However, because the strength of prism is strongly influenced by the number of blocks, the analytical solution based on a unit interlocking block could not well predict the compressive strength of the prism.
2. Laboratory compressive tests are conducted on a series of multiple block prisms. Strong seating effect of the dry-stacking interlocking brick prisms on their compression performance is observed. It is found that the ultimate strength decreases with the increase in the number of blocks because of the increased number of interlocking joints.

3. Detailed numerical models using different contact modelling methods are generated which could reasonably predict the behaviour of interlocking brick prisms. The imperfect contact model gives the closest prediction considering the initial stiffness, the ultimate compressive load-carrying capacity and damage modes. However, none of these methods could replicate the seating effect.
4. Both laboratory tests and numerical simulation reveal the damage and failure patterns of interlocking brick prisms.
5. Parametric study quantifies the influence of the number of bricks, joint roughness amplitudes and material compressive strength on the prism compressive capacity. A modified formula is derived to predict the compressive strength of interlocking brick prisms with consideration of the number of blocks, joint roughness amplitudes, and material strength. And a semi-empirical prediction method is also derived to predict the axial stiffness of the interlocking brick prisms.

Acknowledgments

The authors would like to acknowledge the financial support from Australian Research Council under LP170100846 provided by Tetraloc Pty Ltd for carrying out this study.

Reference

[1] Giamundo V, Lignola G, Maddaloni G, Da Porto F, Prota A, Manfredi G. Shaking table tests on a full-scale unreinforced and IMG-retrofitted clay brick masonry barrel vault. Bulletin of Earthquake Engineering. 2016;14:1663-93.
[2] Ngapeya GGC, Waldmann D, Scholzen F. Impact of the height imperfections of masonry blocks on the load bearing capacity of dry-stack masonry walls. Construction and Building Materials. 2018;165:898-913.
[3] Bui TT, Limam A, Sarhosis V, Hjiaj M. Discrete element modelling of the in-plane and out-of-plane behaviour of dry-joint masonry wall constructions. Engineering Structures. 2017;136:277-94.
[4] Casapulla C, Mousavian E, Zarghani M. A digital tool to design structurally feasible semi-circular masonry arches composed of interlocking blocks. Computers & Structures. 2019;221:111-26.
[5] Dyskin AV, Pasternak E, Estrin Y. Mortarless structures based on topological interlocking. Frontiers of Structural and Civil Engineering. 2012;6:188-97.
[6] Liu H, Liu P, Lin K, Zhao S. Cyclic behavior of mortarless brick joints with different interlocking shapes. Materials. 2016;9:166-78.
[7] Sturm T, Ramos LF, Lourenço PB. Characterization of dry-stack interlocking compressed earth blocks. Materials and Structures. 2015;48:3059-74.
[8] Ali M. Use of coconut fibre reinforced concrete and coconut-fibre ropes for seismic-resistant construction. Materiales de Construcción. 2016;66:073.
[9] Thanoon WA, Jaafar MS, Kadir MRA, Ali AAA, Trikha D, Najm AM. Development of an innovative interlocking load bearing hollow block system in Malaysia. Construction and Building Materials. 2004;18:445-54.
[10] Bragança L, Pinheiro M. Portugal SB10: sustainable building affordable to all: low cost sustainable solutions. Portugal SB10: sustainable building affordable to all: low cost sustainable solutions: Universidade do Minho; 2010. p. 1-870.

[11] Edwards J, Gayed M, Pyra M, Rodriguez T. Design and Construction of Interlocking Mortarless Block Masonry. 2 nd Masonry Mini Symposium demonton, Alberta 2010. p. 4-43.
[12] Gallegos H. Mortarless masonry: the Mecano system. International Journal of Housing Science and its Applications. 1988;12:145-57.
[13] Drysdale RG, Gazzola EA. Strength and deformation properties of a grouted, dry-stacked, interlocking, concrete block system. Brick and Block Masonry. 1991;1:164-71.
[14] Jaafar MS, Thanoon WA, Najm AM, Abdulkadir MR, Ali AAA. Strength correlation between individual block, prism and basic wall panel for load bearing interlocking mortarless hollow block masonry. Construction and Building Materials. 2006;20:492-8.
[15] Drysdale RG, Eng P. Properties of AZAR dry-stack block-IV™ construction. Hamilton, Ontario: McMaster University; 2005.
[16] Anand KB, Ramamurthy K. Development and evaluation of hollow concrete interlocking block masonry system. The Masonry Society Journal. 2005;23:11-9.
[17] Al-Fakih A, Mohammed BS, Liew MS. Behavior of the Dry Bed Joint in the Mortarless Interlocking Masonry System: an Overview. Civil Engineering Research Journal. 2018;4:1-5.
[18] Anand KB, Ramamurthy K. Development and performance evaluation of interlocking-block masonry. Journal of Architectural Engineering. 2000;6:45-51.
[19] Ramamurthy K, Kunhanandan Nambiar EK. Accelerated masonry construction review and future prospects. Progress in Structural Engineering and Materials. 2004;6:1-9.
[20] Wang G, Li Y, Zheng N, Ingham JM. Testing and modelling the in-plane seismic response of clay brick masonry walls with boundary columns made of precast concrete interlocking blocks. Engineering Structures. 2017;131:513-29.
[21] Alwathaf AH, Thanoon WA, Jaafar MS, Noorzaei J, Kadir MRA. Shear characteristic of interlocking mortarless block masonry joints. Masonry International. 2005;18:39-44.
[22] Oikonomopoulou F, Bristogianni T, Barou L, Jacobs E, Frigo G, Veera FA et al. Interlocking cast glass components, Exploring a demountable dry-assembly structural glass system. Heron. 2018;63:103.
[23] Ali M, Gultom RJ, Chouw N. Capacity of innovative interlocking blocks under monotonic loading. Construction and Building Materials. 2012;37:812-21.
[24] Tang Z, Ali M, Chouw N. Residual compressive and shear strengths of novel coconut-fibre-reinforced-concrete interlocking blocks. Construction and Building Materials. 2014;66:533-40.
[25] Rekik A, Allaoui S, Gasser A, Blond E, Andreev K, Sinnema S. Experiments and nonlinear homogenization sustaining mean-field theories for refractory mortarless masonry: The classical secant procedure and its improved variants. European Journal of Mechanics-A/Solids. 2015;49:67-81.
[26] Thanoon WA, Alwathaf AH, Noorzaei J, Jaafar MS, Abdulkadir MR. Nonlinear finite element analysis of grouted and ungrouted hollow interlocking mortarless block masonry system. Engineering Structures. 2008;30:1560-72.
[27] Ayed HB, Limam O, Aidi M, Jelidi A. Experimental and numerical study of Interlocking Stabilized Earth Blocks mechanical behavior. Journal of Building Engineering. 2016;7:207-16.
[28] Jaafar MS, Alwathaf AH, Thanoon WA, Noorzaei J, Abdulkadir MR. Behaviour of interlocking mortarless block masonry. Proceedings of the Institution of Civil Engineers-Construction Materials. 2006;159:111-7.
[29] Lee YH, Shek PN, Mohammad S. Structural performance of reinforced interlocking blocks column. Construction and Building Materials. 2017;142:469-81.
[30] Zhang X, Hao H, Zheng J, Hernandez F. The mechanical performance of concrete shear key for prefabricated structures. Advances in Structural Engineering. 2020:1369433220950618.
[31] Sokairge H, Rashad A, Elshafie H. Behavior of post-tensioned dry-stack interlocking masonry walls under out of plane loading. Construction and Building Materials. 2017;133:348-57.
[32] Li C, Hao H, Bi K. Numerical study on the seismic performance of precast segmental concrete columns under cyclic loading. Engineering Structures. 2017;148:373-86.
[33] Li C, Hao H, Zhang X, Bi K. Experimental study of precast segmental columns with unbonded tendons under cyclic loading. Advances in Structural Engineering. 2017:319-34.
[34] Zhang X, Hao H, Li M, Zong Z, Bruechert JW. The blast resistant performance of concrete-filled steel-tube segmental columns. Journal of Constructional Steel Research. 2020;168:105997.
[35] Zhang X, Hao H. Improved impact resistant capacity of segmental column with fibre reinforced polymer wrap. International Journal of Impact Engineering. 2019;125:117-33.

[36] Zhang X, Hao H, Li C, Van Do T. Experimental study on the behavior of precast segmental column with domed shear key and unbonded Post-Tensioning tendon under impact loading. Engineering Structures. 2018;173:589-605.

[37] Zhang X, Hao H, Li C. The effect of concrete shear key on the performance of segmental columns subjected to impact loading. Advances in Structural Engineering. 2017;20:352-73.

[38] Beall C. New masonry products and materials. Progress in Structural Engineering and Materials. 2000;2:296-303.

[39] Murray EB. Dry Stacked Surface Bonded Masonry-Structural Testing and Evaluation. 2007.

[40] Agaajani S, Waldmann D. Stabilité de systèmes de murs en blocs de béton emboîtables sans joints en mortier. 2012.

[41] Agaajani S. Development and Investigation of a New Dry-Stacked Wall System: University of Luxembourg, Luxembourg, Luxembourg; 2015.

[42] Casapulla C, Portioli F. Experimental tests on the limit states of dry-jointed tuff blocks. Materials and Structures. 2016;49:751-67.

[43] Buyukozturk O, Bakhoum MM, Michael Beattie S. Shear behavior of joints in precast concrete segmental bridges. Journal of Structural Engineering. 1990;116:3380-401.

[44] Zahra T, Dhanasekar M. Characterisation and strategies for mitigation of the contact surface unevenness in dry-stack masonry. Construction and Building Materials. 2018;169:612-28.

[45] Yang GM, Coquille JC, Fontaine JF, Lambertin M. Contact pressure between two rough surfaces of a cylindrical fit. Journal of Materials Processing Technology. 2002;123:490-7.

[46] Bolhassani M, Hamid AA, Lau ACW, Moon F. Simplified micro modeling of partially grouted masonry assemblages. Construction and Building Materials. 2015;83:159-73.

[47] Bosro MZM, Samad AAA, Mohamad N, Ali N, Inn GW, Tambichik MA et al. Computational Study of Mortarless Masonry Block System Under Uniaxial Compression Load. International Journal of Integrated Engineering. 2018;10:74-9.

[48] Ngapeya GGC, Waldmann D. Experimental and analytical analysis of the load-bearing capacity Pu of improved dry-stacked masonry. Journal of Building Engineering. 2020;27:100927.

[49] Silva RA, Soares E, Oliveira DV, Miranda T, Cristelo NM, Leitão D. Mechanical characterisation of dry-stack masonry made of CEBs stabilised with alkaline activation. Construction and Building Materials. 2015;75:349-58.

[50] Andreev K, Sinnema S, Rekik A, Allaoui S, Blond E, Gasser A. Compressive behaviour of dry joints in refractory ceramic masonry. Construction and Building Materials. 2012;34:402-8.

[51] Lourenço PB, Oliveira DV, Roca P, Orduña A. Dry joint stone masonry walls subjected to in-plane combined loading. Journal of Structural Engineering. 2005;131:1665-73.

[52] Zahra T, Yin Z, Dhanasekar M. Experimental investigation of dry joint surface and closure characteristics of interlocking blocks under compression. Brick and Block Masonry. 2016:2003-9.

[53] Thanoon WAM, Alwathaf AH, Noorzaei J, Jaafar MS, Abdulkadir MR. Finite element analysis of interlocking mortarless hollow block masonry prism. Computers & Structures. 2008;86:520-8.

[54] Safiee NA, Jaafar MS, Alwathaf AH, Noorzaei J, Abdulkadir MR. Structural behavior of mortarless interlocking load bearing hollow block wall panel under out-of-plane loading. Advances in structural engineering. 2011;14:1185-96.

[55] Mousavian E, Casapulla C. Structurally informed design of interlocking block assemblages using limit analysis. Journal of Computational Design and Engineering. 2020.

[56] Thompson MK. Methods for generating rough surfaces in ANSYS. Proceedings of the 2006 International ANSYS Users Conference & Exhibition, Pittsburgh, PA2006.

[57] Thompson MK, Thompson J. Methods for generating probabilistic rough surfaces in ANSYS. Proc 20th Korea ANSYS User's Conf2010. p. 9-10.

[58] Thompson MK. A comparison of methods to evaluate the behavior of finite element models with rough surfaces. Scanning. 2011;33:353-69.

[59] Wong RHC, Chau KT, Tang CA, Lin P. Analysis of crack coalescence in rock-like materials containing three flaws—part I: experimental approach. International Journal of Rock Mechanics and Mining Sciences. 2001;38:909-24.

[60] Zhang K, Cao P, Ma G, Wang W, Fan W, Li K. Strength, fragmentation and fractal properties of mixed flaws. Acta Geotechnica. 2016;11:901-12.

[61] Wong RHC, Chau KT. Crack coalescence in a rock-like material containing two cracks. International Journal of Rock Mechanics and Mining Sciences. 1998;35:147-64.
[62] Tasdemir MA, Maji AK, Shah SP. Crack propagation in concrete under compression. Journal of engineering mechanics. 1990;116:1058-76.
[63] Wu Z, Zhao G, Huang C. Fracture toughness and fracture energy for different concrete strength. Journal of Dalian University of technology. 1993;33:73-7.
[64] ASTM. Standard test methods for sampling and testing concrete masonry units and related units. 2008.
[65] EN C. 1052-1: Methods of test for masonry, Part 1: Determination of compressive strength. British Standards Institution, London. 1999.
[66] Systèmes D. ABAQUS Documentation (Dassault Systèmes, Providence, RI). Version; 2014.
[67] Lubliner J, Oliver J, Oller S, Oñate E. A plastic-damage model for concrete. International Journal of solids and structures. 1989;25:299-326.
[68] Simulia. Abaqus Analysis User's Guide, Version 6.14. Dassault Systemes Providence, RI; 2014.
[69] Martínez M, Atamturktur S, Ross B, Thompson J. Assessing the Compressive Behavior of Dry-Stacked Concrete Masonry with Experimentally Informed Numerical Models. Journal of Structural Engineering. 2018;144:04018080.
[70] Prabhu S, Atamturktur S, Brosnan D, Messier P, Dorrance R. Foundation settlement analysis of Fort Sumter National Monument: Model development and predictive assessment. Engineering Structures. 2014;65:1-12.
[71] Gorst NJS, Williamson SJ, Pallett PF, Clark LA. Friction in temporary works. Research Rep. 2003;71.
[72] Vasconcelos G, Lourenço PB. Experimental characterization of stone masonry in shear and compression. Construction and Building Materials. 2009;23:3337-45.
[73] Park CH, Bobet A. Crack coalescence in specimens with open and closed flaws: a comparison. International Journal of Rock Mechanics and Mining Sciences. 2009;46:819-29.
[74] Ashby MF, Hallam SD. The failure of brittle solids containing small cracks under compressive stress states. Acta Metallurgica. 1986;34:497-510.
[75] Sarhat SR, Sherwood EG. The prediction of compressive strength of ungrouted hollow concrete block masonry. Construction and Building Materials. 2014;58:111-21.